AGU100 ADVANCING EARTH AND SPACE SCIENCE

Geochemistry, Geophysics, Geosystems

RESEARCH ARTICLE
10.1029/2018GC007539

Constraining Instantaneous Fluxes and Integrated Compositions of Fluvially Discharged Organic Matter

Chantal V. Freymond[1], Maarten Lupker[1], Francien Peterse[1,2], Negar Haghipour[1], Lukas Wacker[3], Florin Filip[4,5], Liviu Giosan[6], and Timothy I. Eglinton[1]

[1]Geological Institute, ETH Zürich, Zürich, Switzerland, [2]Department of Earth Sciences, Utrecht University, Utrecht, Netherlands, [3]Ion Beam Physics, ETH Zürich, Zürich, Switzerland, [4]Institute for Fluvial and Marine Systems, Bucharest, Romania, [5]Fabrica de Cercetare, Romania Woods Hole, MA, USA, [6]Woods Hole Oceanographic Institution, Woods Hole, MA, USA

Abstract Fluvial export of organic carbon (OC) and burial in ocean sediments comprises an important carbon sink, but fluxes remain poorly constrained, particularly for specific organic components. Here OC and lipid biomarker contents and isotopic characteristics of suspended matter determined in depth profiles across an active channel close to the terminus of the Danube River are used to constrain instantaneous OC and biomarker fluxes and integrated compositions during high to moderate discharges. During high (*moderate*) discharge, the total Danube exports 8 (*7*) kg/s OC, 7 (*3*) g/s higher plant-derived long-chain fatty acids (LCFA), 34 (*21*) g/s short-chain fatty acids (SCFA), and 0.5 (*0.2*) g/s soil bacterial membrane lipids (brGDGTs). Integrated stable carbon isotopic compositions were TOC: −28.0 (−*27.6*)‰, LCFA: −33.5 (−*32.8*)‰ and Δ^{14}C TOC: −129 (−*38*)‰, LCFA: −134 (−*143*)‰, respectively. Such estimates will aid in establishing quantitative links between production, export, and burial of OC from the terrestrial biosphere.

Key Points:
- Bulk organic carbon and biomarker concentrations as well as structural and isotopic composition were measured in depth profiles across a major river
- This data set, characterizing the suspended particulate matter, was combined with Acoustic Doppler Current Profiler water velocity data
- Cross-section integrated suspended matter composition and instantaneous organic carbon and biomarker fluxes were calculated

Supporting Information:
- Supporting Information S1
- Data Set S1

Correspondence to:
C. V. Freymond,
chantal.freymond@erdw.ethz.ch

Citation:
Freymond, C. V., Lupker, M., Peterse, F., Haghipour, N., Wacker, L., Filip, F., et al. (2018). Constraining instantaneous fluxes and integrated compositions of fluvially discharged organic matter. *Geochemistry, Geophysics, Geosystems*, *19*, 2453–2462. https://doi.org/10.1029/2018GC007539

Received 12 MAR 2018
Accepted 8 MAY 2018
Accepted article online 7 JUN 2018
Published online 11 AUG 2018

1. Introduction

Rivers are the most important conduits for transfer of sediment eroded on continents to ocean basins. Globally, rivers discharge about 19 billion tons of sediment per year to the coastal ocean (Milliman & Farnsworth, 2011), entraining and exporting about 200 Mt/yr particulate organic carbon (POC; Galy et al., 2015). Once deposited on continental margins, the OC may be stored on long timescales, and corresponding sedimentary sequences thus serve both as long-term sink for terrigenous OC and as continuous archives of paleoenvironmental change in the adjacent river catchments.

Global estimates for riverine discharge of suspended particulate matter (SPM) are not well constrained because of variable sampling strategies and frequencies over different hydrological conditions (Milliman & Farnsworth, 2011). Often, such estimates stem from measurement of near-surface SPM close to the river axis, and assumptions are then made concerning the homogeneity of the suspended load in order to derive an integrated flux. However, the vertical distribution of SPM in a river is influenced by hydrodynamic sorting, which causes coarser and higher-density sediment to be transported closer to the riverbed, whereas finer and low-density particles are more homogeneously distributed over the water column (Bouchez et al., 2011; Lupker et al., 2011). Several studies have explored variations in the distribution and the mineral and inorganic geochemical characteristics of SPM across depth and cross sections of rivers in order to derive integrated SPM fluxes (e.g., Armijos et al., 2017; Bouchez et al., 2011; Lupker et al., 2011). In contrast, the lateral and vertical variability in bulk OC (Bouchez et al., 2014; Galy et al., 2008; Goni et al., 2005; Guinoiseau et al., 2016) and molecular (biomarker) (Feng et al., 2016) composition and corresponding isotopic (stable and radiocarbon) characteristics are significantly less well known. This is in part due to logistical challenges associated with sampling and analysis for trace organic constituents, hindering our ability to place robust constraints on the characteristics and fluxes of POC and biomarkers discharged to the oceans.

In a recent study, the existence of a POC-rich and particulate lignin-rich suspended sediment layer just above the riverbed was observed in the Madre de Dios River, and was attributed to high proportions of plant debris at this particular depth (Feng et al., 2016). In contrast, soil OC is thought to be mainly associated with fine-grained phyllosilicates (Baldock & Skjemstad, 2000; Doetterl et al., 2015; Freymond et al., 2018), that are well dispersed throughout the water column and therefore more uniform vertical distributions are expected (Bouchez et al., 2011).

In this study, SPM was characterized from several depth profiles that serve as a "picket fence" spanning one of the two main branches of the Danube River at the apex prior of the delta. Bulk OC and biomarker concentrations as well as corresponding stable and radiocarbon isotopic compositions of SPM samples collected on campaigns during two different years were determined, and compared to adjacent river sediment deposits. Focus was placed on long-chain fatty acids (LCFA) and branched glycerol dialkyl glycerol tetraethers (brGDGTs) as tracers of higher plant-derived material (Eglinton & Eglinton, 2008) and soil OC (Schouten et al., 2013), respectively, in order to constrain the instantaneous export flux of OC and these source-specific biomarkers to the Black Sea. Extrapolating bulk and compound-specific isotope signatures as well as proxy values to the river cross section, we assess heterogeneity in organic matter (OM) associated with SPM and potential uncertainties associated with extrapolation of single-point measurements to derive estimates of fluvial discharge.

2. Site Description

The Danube River, with a catchment area of 817,000 km^2, including parts of the Eastern Alps, the Carpathian, Dinaric, and Balkan mountains, and large sedimentary basins (Vienna basin, Pannonian, and lower Danubian plains; Schiller et al., 2010), is the second largest fluvial system in Europe. Mean annual discharge to the Black Sea is 6,850 m^3/s (Schiller et al., 2010), peak flow occurs in spring with monthly average discharges reaching ca. 9,000 m^3/s, while minimum monthly averaged discharges reach 4,500 m^3/s in autumn (GRDC). Present-day total sediment export (SPM and bed load) is 25–35 Mt/yr, of which about 18 Mt/yr is in the suspended fraction (Habersack et al., 2016). At the beginning of its delta, the Danube main stem splits into two main branches—the northern Chilia branch and southern Tulcea branch. The Tulcea branch further splits into the Sulina and Sf. Gheorge branches (supporting information Figure S1).

Samples were collected on the Tulcea branch that accounts for 45% of the total water flux (Torica, 2006), shortly downstream of the diffluence (<2 km) (supporting information Figure S1). For political reasons, depth profiles could not be taken across the entire Danube main stem before its main diffluence as it coincides with the Romanian-Ukrainian border. However, it is assumed given its proximity to the main stem that the SPM is representative of material entering from the river to the delta. Furthermore, the sampling location is >50 km downstream of the last large tributary confluence, and therefore, the river is expected to be well mixed.

3. Methods

3.1. Sample Collection

Sampling took place in early June 2013 and early September 2014 during decreasing water level (supporting information Figure S2). Water depth, bathymetry, velocity, and total discharge were determined by deployment of an Acoustic Doppler Current Profiler (ADCP). Based on the ADCP river cross sections, optimal locations for the depth profiles and large-volume water sampling were determined (supporting information Figure S4). Water samples were collected with a 5 L horizontal, open ended, sampling bottle equipped with a pneumatic closing mechanism (Lupker et al., 2011). The depth of the sampling bottle was controlled with an echo sounder. In 2013, about 30 L of water was sampled for each depth at the middle profile and about 10 L at the left and right profiles, as well as the near shore surface water locations. In 2014, >60 L water was sampled for every profile and depth. Water samples were filtered over precombusted and preweighted glass fiber filters (90 mm, 0.7 μm GF/F filters, Whatman). About 10 L of each sample was filtered over membrane filters (90 mm, 0.22 μm PES filters, Membrane Solutions) but not examined in this study. Filters were stored at −20°C until they were freeze-dried. At the location of the sampling transect, fine-grained (<1 mm) sediment that was recently deposited on the riverbanks was collected from the shore (Freymond et al., 2017). Subsequently, the term "river sediment" is used for these fresh deposits.

3.2. ADCP Acquisition and Data Processing

The ADCP (Rio Grande, 1,200 kHz) was mounted to the side of a boat ca. 0.1 m below the water surface (e.g., Muste et al., 2004). Riverbed geometry, water discharge, and velocity profiles were determined with multiple river crossings perpendicular to the flow in bottom track mode with a vertical resolution of 0.1/0.25 m (2013/2014, respectively).

In 2014, a GPS unit was connected to the ADCP to record the exact transect position. Comparison between the bottom and GPS-referenced velocity did not reveal the presence of a moving bed (Callede et al., 2000). Four transects in the direct vicinity of the sediment sampling points were averaged using the USGS Velocity Mapping Toolbox (Parsons et al., 2013). These transects closely agree and the discharge calculated for each individual transect does not vary by more than 10%. In 2013, no GPS was available, making precise transect averaging impossible. A single river transect was selected (out of seven; discharge estimates varied by $<$6%) based on data quality and proximity to the 2013 water sampling points, and used for calculations.

The velocity data were further processed in R (R Core Team, 2014). Missing discharge data were interpolated based on the average of neighboring velocity profiles. The top and bottom discharge data that cannot be resolved by the ADCP was extrapolated based on a power law fit to the available velocity data (Chen, 1991; supporting information Figure S4). Discharge was calculated based on the velocity data and corrected for the difference between ship and water flow direction.

Concentration and proxy data from the depth profiles were extrapolated to the river cross section using an inverse distance method. These extrapolated data were then combined with the water discharge profiles to derive discharge-weighted proxy average values and instantaneous fluxes of OC and biomarkers.

3.3. Bulk Measurements: SPM Concentration, TOC, $\delta^{13}C$, ^{14}C

To determine SPM concentrations, precombusted filters were weighted before and after filtering a known amount of water and subsequent freeze-drying. SPM concentrations are reported in mg/L.

For total organic carbon (TOC), $\delta^{13}C$ and ^{14}C measurement, filter pieces of known diameter, and river sediments were decarbonated as described in Freymond et al. (2018). Blank filters were treated with the same method. The measurement was performed on a coupled EA-IRMS-AMS (elemental analyzer, isotope ratio mass spectrometer, accelerator mass spectrometer) system (McIntyre et al., 2016) and corrected for procedural blank values.

3.4. FA and brGDGT Extraction and Quantification

Freeze-dried filters were cut in pieces whereas river sediments were sieved to $<$63 μm prior to microwave extraction. brGDGTs were extracted as described in Freymond et al. (2017) and measured on a UHPLC-APCI-MS system (Ultra High Performance Liquid Chromatograph, Agilent 1290, coupled to a quadrupole Mass Spectrometer, Agilent 6310) at Utrecht University following the settings of Hopmans et al. (2016). For proxy calculations, see supporting information equation (S1) and Figure S3.

FAs were extracted as described in Freymond et al. (2018) from the same total lipid extract as for the brGDGTs and quantified against an external standard (*n*-$C_{4–24}$ even carbon saturated FAMEs; Supelco) on a gas chromatograph equipped with a flame ionization detector (GC-FID; Agilent 7890A). Results are reported as sum of even C-number long-chain FA (*n*-$C_{24–30}$; LCFA) and short-chain FA (*n*-$C_{16–18}$; SCFA) concentrations.

3.5. LCFA $\delta^{13}C$ Measurement

LCFA $\delta^{13}C$ determination was performed in duplicate measurements with a GC-IRMS (gas chromatograph, Thermo Trace GC Ultra, coupled to an isotope ratio mass spectrometer, Thermo Delta V Plus). The $\delta^{13}C$ values were calibrated using an external fatty acid methyl ester standard calibrated to the VPDB scale, and corrected for carbon atoms that were added during methylation. Results are shown as concentration weighted average values (*n*-$C_{24–30}$) with standard deviations ranging from 0.12‰ to 0.97‰.

3.6. Compound-Specific FA ^{14}C Measurement

Due to the low abundance of LCFAs (generally $<$1 μg/L), samples from different depths and profiles were combined in order to obtain sufficient C required for ^{14}C measurement (typically $>$10 μgC) (supporting information Figure S5). Separation and isolation of FAs were achieved using a preparative capillary gas chromatograph (PCGC; Eglinton et al., 1996). FAs *n*-C_{16}, *n*-C_{18}, and *n*-$C_{24–30}$ were collected in three separate traps. Two blank runs with the same amount of single runs and the same time windows of collection as for samples were run to determine the processing blank. The single compounds and blanks were run over SiO_2 columns to remove any contamination by column bleed. Then, the single compounds and blanks were converted to CO_2 with precombusted CuO in evacuated quartz tubes (850°C, 5 h). ^{14}C on the sample and blank CO_2 was measured with a MICADAS (Mini radiocarbon Dating System; Christl et al., 2013; Synal et al., 2007) at the Laboratory for Ion Beam Physics at ETH. Fraction modern (Fm) values were corrected for the

processing blank after Shah and Pearson (2007) ($F^{14}C = 0.17 \pm 0.03$; mass of contamination: 0.31 ± 0.09 μg) and for carbon atoms added during methylation. Fm values were subsequently converted to $\Delta^{14}C$ values (Sternström et al., 2011).

4. Results

4.1. Depth Profiles

SPM concentrations range from 25 to 70 mg/L and do not show a clear variation with depth (Figure 1). However, SPM concentrations are higher in the middle profile than in the right and left profiles in 2014, whereas the opposite is the case in 2013. TOC contents, ranging between 1.3% and 2.4%, show a maximum at middepth, which is most pronounced in the middle profile in 2014. LCFA, SCFA, and brGDGT concentrations are higher in 2013 than 2014, ranging from 0.37 to 0.98 and 0.19–0.54 μg/L for LCFAs, 1.91–5.40 and 1.22–4.64 μg/L for SCFAs; and 26.59–62.55 and 12.83–40.56 ng/L for brGDGTs in 2013 and 2014, respectively. LCFA and brGDGT concentrations are strongly correlated (0.95, Pearson correlation coefficient). Bulk $\delta^{13}C$ values are relatively constant over different locations along the river cross section, depths and years with a statistical (i.e., not discharge-weighted) average value of $-27.8‰$ ($\pm 0.34‰$, n = 23) after excluding two outliers (2013 right 5 m = $-36.3‰$, and 2014 middle surface = $-19.1‰$). Bulk $\Delta^{14}C$ values are relatively homogeneous in 2013, ranging from $-155‰$ to $-90‰$ (average $-126 \pm 18‰$, n = 12). In 2014, bulk $\Delta^{14}C$

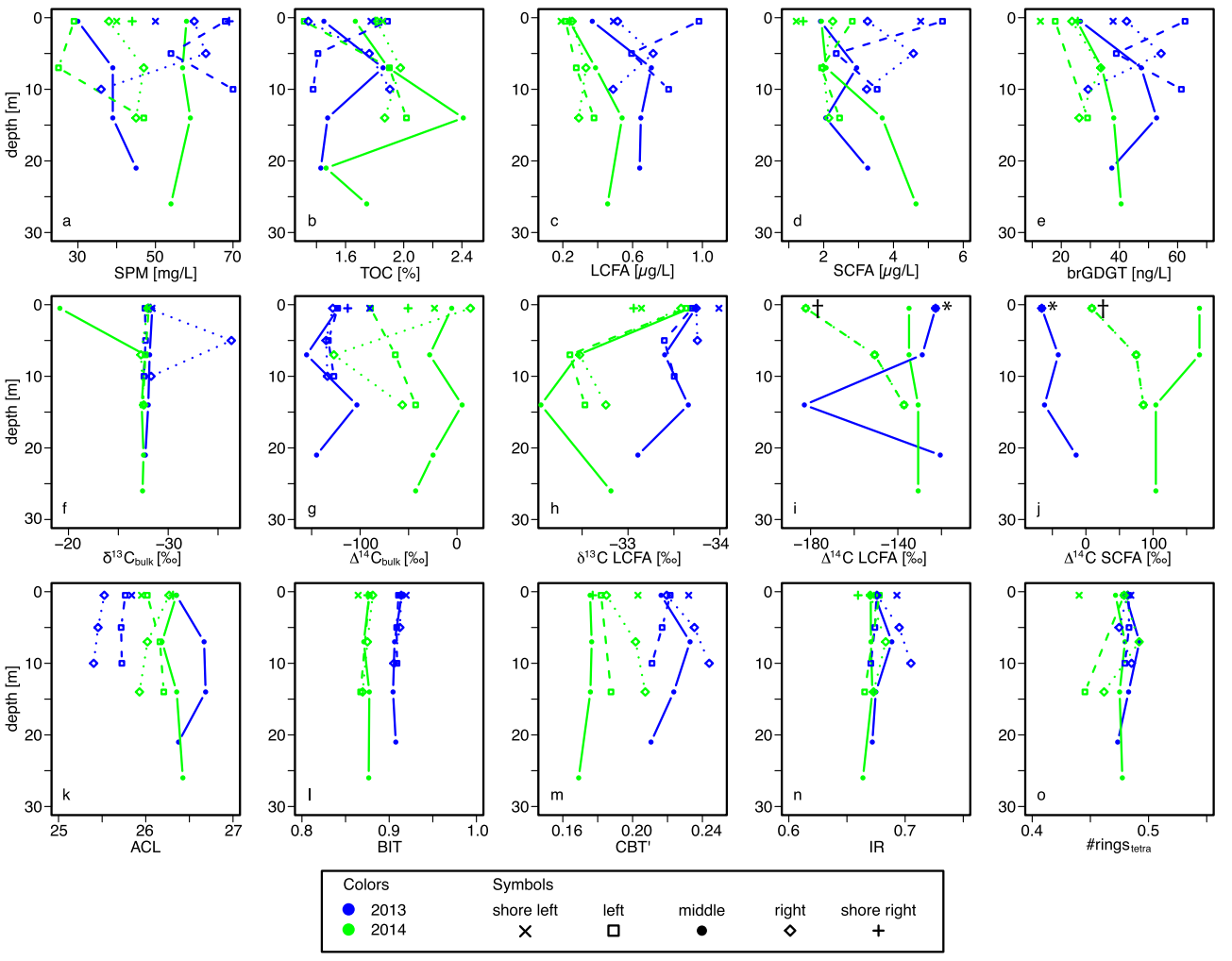

Figure 1. Concentration and proxy values in depth profiles. Solid lines show the middle; dashed lines the left and right profiles. For FA ^{14}C measurement, the surface samples from the left, middle, and right profiles in 2013 were combined into one sample and marked with an (*). In 2014, samples of the respective depths from left and right profiles were combined (surface left + right; 7 m left + right; 14 m left + right) and marked with a (†) (supporting information Figure S5).

Table 1
Discharge-Weighted Average OC and Biomarker Proxy Values in SPM and River Sediments

	River cross section SPM		River bar sediment	
	2013	2014	2013	2014
TOC (%)	1.6	1.8	0.9[a]	0.7[a]
Bulk $\delta^{13}C$ (‰)	−28.0	−27.6	−27.3	−26.0
Bulk $\Delta^{14}C$ (‰)	−129	−38	−224	−240
LCFA $\delta^{13}C$ (‰)	−33.5	−32.8	−33.5	−33.0
LCFA $\Delta^{14}C$ (‰)	−134	−143	−231	−209
SCFA $\Delta^{14}C$ (‰)	−52	99	−18	−46
ACL	26.1	26.2	27.1	27.5
BIT	0.91	0.87	0.91[b]	0.89
CBT′	0.22	0.18	0.03[b]	0.06
MATmr (°C)	9.2	9.9	8.4[b]	8.3
pH	7.5	7.4	7.2[b]	7.2
IR	0.68	0.67	0.55	0.57
$\#rings_{tetra}$	0.48	0.47	0.50	0.47

[a]Data from Freymond et al. (2018). [b]Data from Freymond et al. (2017).

values were higher and slightly more variable, ranging from −127‰ to +14‰ (average −41 ± 38‰, n = 13), with highest values in the middle profile. Compound-specific LCFA $\delta^{13}C$ values of the left, middle, and right profile surface water are similar for both years with an average of −33.7‰ (±0.06‰, n = 6), although surface water from close to the left and right shores show more ^{13}C-enriched values than midchannel in 2014. In 2013, depth profiles exhibit relatively constant LCFA $\delta^{13}C$ values whereas in 2014, values are about 1‰ more enriched at 7–26 m depth than at the surface. LCFA average chain length (ACL) is constant with depth, but shows differences across the river. The middle profile in 2013 shows an average of 26.5 whereas the left and right profiles show an average of 25.7 and 25.5, respectively. In 2014, ACL is only slightly higher in the middle profile (averages: middle = 26.3, left = 26.1, right = 26.0). brGDGT-derived proxies are generally constant with depth. BIT and CBT′ show distinct values between the 2 years, however, the differences are small and corresponding isomer ratio (IR) and $\#rings_{tetra}$ values fall in the same range in 2013 and 2014 (Figure 1).

In general, no significant correlations were found between sample depth and geochemical parameters. brGDGT and LCFA concentrations only display weak correlations with SPM concentration of 0.65 and 0.57, respectively (Pearson correlation coefficients).

4.2. Discharge-Weighted Average and Instantaneous Fluxes

Extrapolated and discharge-weighted average bulk and biomarker proxy values for the 2013 and 2014 samplings are shown in Table 1 (supporting information Figures S6 and S7). Between years, average TOC (1.6/1.8%) and bulk $\delta^{13}C$ (−28.0/−27.6‰; 2013/2014, respectively) are very comparable. Bulk $\Delta^{14}C$ values are more variable, and imply a higher proportion of fossil or preaged OC in 2013 ($\Delta^{14}C = -129‰$) compared to 2014 ($\Delta^{14}C = -38‰$). The distinct changes in LCFA $\delta^{13}C$ values with depth between the 2 years result in a slightly lower average value in 2013 than 2014 (−33.5/−32.8‰), whereas average LCFA $\Delta^{14}C$ values for 2013 and 2014 samples are comparable. Similarly, average brGDGT-derived proxy values show little variation between the two sampling periods (Table 1).

Discharge-weighted instantaneous SPM, OC, and biomarker fluxes for the two sampling periods are shown in Figure 2 and supporting information Table S1.

4.3. River Sediment Composition

River sediment deposits at the location of the depth profiles are characterized by lower TOC content (0.9/0.7; 2013/2014, respectively) and lower bulk (−224/−240‰) and LCFA $\Delta^{14}C$ values (−231/−209‰)

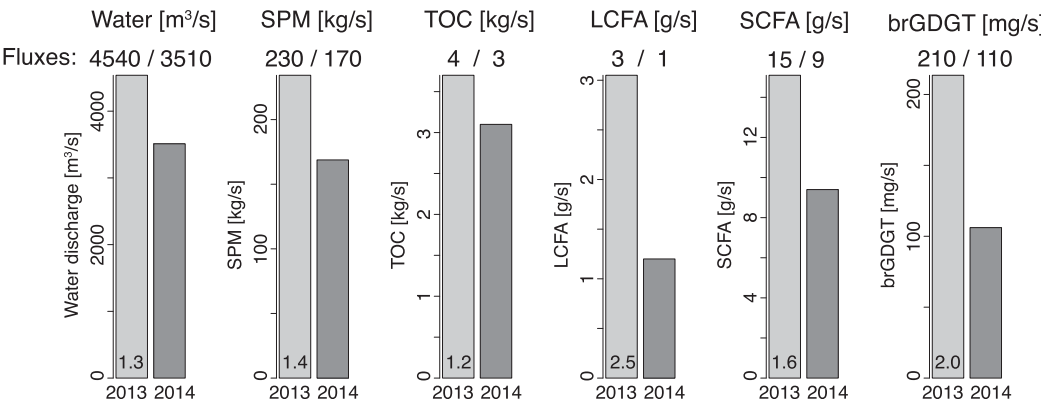

Figure 2. Instantaneous Danube River water, SPM, TOC, and biomarker fluxes in 2013 and 2014. The number in the 2013 bar is the factor by which the 2013 flux is higher than in 2014.

compared to cross-section SPM. Stable isotope and proxy values, except CBT′ that shows significantly lower values in river sediments, are comparable to the ones in SPM samples (Table 1).

5. Discussion

5.1. SPM Composition and Fluxes

The identification of only small variations in concentrations and proxy values with depth and among different profiles across the channel shows that the SPM in the river is well mixed at the sampling location (Figure 1, supporting information Figures S6 and S7). Only SPM concentration and ACL show systematic differences across the river. In 2014, SPM is higher in the middle of the river, where the water velocity is highest and thus theoretically coarser-grained particles can be retained in suspension. However, in 2013, SPM concentration is lower in the middle profile compared to the left and right ones. In 2013, ACL in the middle profile is higher compared to profiles on the river flanks, potentially indicating different LCFA sources. However, such a difference is not reflected in corresponding LCFA $\delta^{13}C$ values. In the vertical direction, an increase of SPM with depth is only observed in the middle profile in 2013. The typical hydrodynamic sorting of sediments leading to an increase in the average grain size toward the bottom of the water column, as observed in other large rivers (Bouchez et al., 2011; Feng et al., 2016; Lupker et al., 2011), does not seem to occur here. The OM composition, expressed in bulk $\delta^{13}C$, LCFA $\delta^{13}C$, LCFA $\Delta^{14}C$, ACL, and brGDGT proxy values (Table 1), remains fairly constant between years. The minor compositional changes between 2013 and 2014 are well within the range of interannual and intraannual fluctuations reported for, e.g., the Tagus, Congo, and Yellow Rivers (Hemingway et al., 2017; Tao et al., 2017; Zell et al., 2014). Given that sampling in 2013 and 2014 was in early and in late summer, respectively, observed minor differences likely reflect seasonal variations. However, given the generally homogenous characteristics as a function of location, depth, and time, these data can be considered representative of the SPM composition in the Danube during yearly high-water conditions.

brGDGTs are ubiquitously produced in soils (Peterse et al., 2012; Weijers et al., 2007), and hence may serve as tracers for soil OC during fluvial transport, even though in situ production in lake and river waters has also been documented (De Jonge et al., 2014b; Tierney & Russell, 2009; Weber et al., 2015). Although the high BIT index values for Danube SPM (0.91/0.87 in 2013/2014, respectively, Table 1) suggest that brGDGTs are mainly soil-derived (Schouten et al., 2013), these high BIT values may also be the result of a large contribution of in-river produced brGDGTs (De Jonge et al., 2014b). To identify such a potential in situ contribution, the IR, which is the fractional abundance of 6-methyl-isomer brGDGTs compared to all 5-methyl-isomer and 6-methyl-isomer brGDGTs (supporting information equation (S1) and Figure S3), may be used, where high values relate to relatively more aquatic brGDGTs (De Jonge et al., 2014b). The IR for the SPM (0.68/0.67 for 2013/2014, Table 1) is slightly higher than for the river sediments (0.55/0.57 for 2013/2014, Table 1), indicating potential in situ production. Indeed, SPM IR values are in the same range as for Danube sediments upstream of the Iron Gate dams, where lower water velocities may have enhanced in situ brGDGT production, albeit to a minor extent (Freymond et al., 2017). This is further supported by long-chain diols in the same Danube sediments along the course of the river, where the increased abundance of the C_{32} 1,15-diol indicates that in situ production takes place, predominantly in the stagnant waters in the Iron Gate reservoir (Lattaud et al., 2018). Effectively, in situ production seems to be low in the flowing water of the main branch, and is potentially even lower during high-water conditions due to increased turbidity. Nevertheless, considering the comparable brGDGT composition in the SPM close to the Black Sea with that in fluvial sediment deposits upstream (Freymond et al., 2017), the vast majority of the brGDGTs appears to be derived from soils with a minor in-river brGDGT contribution. This interpretation of predominantly soil (as opposed to aquatic) source is supported by the strong correlation between brGDGT and LCFA concentrations (0.95, Pearson correlation coefficient) in the SPM.

Water discharge was higher in 2013, and correspondingly SPM, TOC, and biomarker fluxes were also higher than in 2014 (Figure 2). The uncertainty on overall fluxes (TOC and biomarkers) remains difficult to assess as they encompass uncertainties associated with (i) water discharge estimates from the ADCP velocity data, (ii) precise sampling coordinates with respect to the reference river section, (iii) sampled volumes, and (iv) analytical uncertainties on biomarker concentration determinations. These uncertainties are difficult to quantify individually, but the differences between the exported biomarker fluxes exceed the overall uncertainty on concentration measurements suggesting a coherent data set. The SPM and TOC fluxes appear to increase in concert with the water flux (factor 1.3, 1.4, and 1.2 higher in 2013 for water, SPM, and TOC, respectively),

whereas LCFA, SCFA, and brGDGT fluxes increase by factors of 2.5, 1.6, and 2.0, respectively, with higher discharge (Figure 2). This relative enhancement in SCFA and brGDGT compared to LCFA fluxes at lower discharge might indicate in-river production during more quiet conditions. Correspondingly, the higher SCFA and bulk $\Delta^{14}C$ values with lower discharge in 2014 may in turn reflect a greater contribution of fresh terrestrial or aquatic biomass relative to preaged soil or a smaller contribution of fossil OC (Table 1). On the other side, lower bulk $\Delta^{14}C$ values during higher discharge in 2013, indicate proportionally higher inputs of (preaged) soil-derived OM (Cathalot et al., 2010; Rosenheim et al., 2013) and/or fossil OC with correspondingly lower in-river production. LCFA $\Delta^{14}C$ values are relatively low ($\sim$1,160 ^{14}C years) not showing a significant difference between years or varying discharge, indicating that the LCFAs primarily derive from mineral-associated OC that is preaged in soils (Tao et al., 2015; Van der Voort et al., 2017).

5.2. Comparison of SPM to River Sediments

TOC concentrations are significantly higher in SPM than in river sediments (Table 1), potentially reflecting hydrodynamic particle sorting during, or decomposition subsequent to, deposition. Higher-density coarse-grained particles (including mineral grains with little associated OC), are preferentially deposited compared to minerals in the clay and fine silt fraction that exhibit a high mineral-specific surface area (SA) available for organomineral interactions (Keil & Mayer, 2014). Additionally, low-density plant debris may preferentially remain in the suspended load. Greater contributions of plant debris to SPM relative to river sediments would also explain the higher bulk OC and LCFA $\Delta^{14}C$ values (i.e., fresher material) of the former (Table 1). Preferential postdepositional degradation of fresher and more labile nonmineral-associated OM in river sediments could also explain the lower TOC values and lower TOC and LCFA $\Delta^{14}C$ values (older ages) of river sediments. However, since LCFA $\delta^{13}C$ values show no indication for enrichment due to degradation (Li et al., 2017; Wang et al., 2016), suggesting a similar origin for LCFAs in SPM and river sediments, we suspect that preferential transport and deposition of mineral-associated LCFAs is the most likely explanation. The lower ACL values for SPM than river sediments are the only indication of additional sources of *n*-C_{24}-FAs to SPM, whereas brGDGT proxy values (BIT, #$rings_{tetra}$) are very comparable. One exception is the higher relative proportion of 6-methyl compared to 5-methyl brGDGT isomers in SPM (reflected in higher CBT′ and slightly higher IR values) than in river sediments, suggesting a small additional aquatic 6-methyl brGDGT source in the river SPM (De Jonge et al., 2014b). On the other hand, corresponding MATmr and pH proxy values are only slightly higher for the SPM (0.8/1.6°C, 0.3/0.2 pH units in 2013/2014, respectively), with these differences being well within the calibration uncertainty (errors: MATmr = 4.6°C; pH = 0.5; De Jonge et al., 2014a). The broad similarity in brGDGT distributions is consistent with the finding of similar brGDGT distributions across different grain size classes in river sediments (Peterse & Eglinton, 2017).

Although the absolute concentration of TOC in SPM is higher than in river sediments, TOC may be comparable in SPM and river sediments when normalized to SA (Freymond et al., 2018). Although the limited sample sizes precluded SA determinations for Danube SPM, Bouchez et al. (2014) found that OC loadings on Amazon River SPM fall within a range typical for riverine suspended sediment (Blair & Aller, 2012). Assessments of loadings may therefore compensate for hydrological sorting processes during SPM deposition on (as well as erosion from) riverbanks.

Overall, taking into account all determined proxies as well as bulk and compound-specific stable and radiocarbon isotopes, we conclude that for a well-mixed large river such as the Danube close to its terminus, the composition of river sediments largely reflects the average SPM composition, albeit with some differences stemming from either hydrodynamic sorting or postdepositional degradation. Nevertheless, for accurate flux assessments, concentrations need to be measured on SPM samples given the significantly lower OC contents of river sediments.

5.3. Implications for OC Export to the Black Sea

Taking into consideration that the Tulcea branch accounts for $\sim$45% of the total Danube discharge, all fluxes were upscaled to 100% to derive fluxes for the entire river as it enters the delta. This results in a water discharge of 10,100/7,800 m^3/s (2013/2014, respectively), significantly above the average yearly discharge of 6,486 m^3/s in both years (Sommerwerk et al., 2009). In 2013, the discharge was close to the average annual flood discharge of 10,889 m^3/s. During these conditions, the total Danube is calculated to export 8/7 kg/s OC, 7/3 g/s LCFAs, 34/21 g/s SCFAs, and 0.5/0.2 g/s brGDGTs (2013/2014, respectively, supporting information Table S1). Extrapolation of these instantaneous SPM fluxes to a yearly sediment discharge yields values of 16/12 Mt/yr of suspended

sediment, which is close to the 18 Mt/yr estimated for the Danube (for 1985–2000) by Habersack et al. (2016). The fact that the two sampling periods correspond to higher than average flow conditions for the Danube may bias the integrated flux estimates by not taking into account low-flow periods with potentially different compositions. However, as mentioned above, the compositional variability of OC is limited over the two discharge regimes that were sampled, suggesting that this bias is likely limited. Furthermore, the sediment load and associated POC flux in rivers are dominated by the export during high flow conditions (e.g., Cathalot et al., 2013; Clark et al., 2017; Smith et al., 2013), making these hydrological periods more representative of yearly averaged fluxes. Upscaling the two studied sections to the entire Danube is therefore reasonable even though it does not take into account the entire flow regimes.

Discharge-weighted SPM bulk $\delta^{13}C$ ($-28.0/-27.6‰$) and $\Delta^{14}C$ ($-129/-38‰$) values (Table 1) are, respectively, lower and higher than those of Black Sea surface sediments and coastal water SPM close to the outflow of the Sulina branch (Kusch et al., 2010; Saliot et al., 2002). Kusch et al. (2010) indicate that Black Sea sediment OC at 18 m water depth already comprises a substantial marine contribution, which is indicated by the lower BIT index (0.64) than for the Danube SPM (0.91/0.87 in 2013/2014, respectively; Table 1). Also, the higher bulk $\delta^{13}C$ value of $-25.7‰$ ($+2.1‰$ on average) points toward a rapid marine overprint of the fluvial signal. Finally, higher bulk OC ages in the marine sediments are counter-intuitive but may be due to hydrological sorting and winnowing (Wakeham et al., 2009) and preferential accumulation of mineral-bound OC (soil or fossil OC) at the studied location (whereas fresh plant debris with lower density might be deposited further offshore) or to postdepositional (e.g., bioturbation) processes that vertically mix sediment of different ages. The discharge-weighted ^{14}C age of the LCFAs discharged in Danube SPM, which is similar for both years of sample collection (ave., 1,140 yr) is comparable to that in Black Sea surface sediments (FA n-$C_{26–30}$ = 1,649 yr; Kusch et al., 2010).

6. Conclusions

To our knowledge, this constitutes the first study that investigates cross-sectional variations in compound-specific stable and radiocarbon isotopic composition of SPM and reports corresponding estimates of biomarker discharge and discharge-weighted isotopic values.

Results show that Danube River SPM is well mixed with minor compositional changes with depth or across the river. Determining OC and biomarker fluxes from one point-sample compared to the picket fence approach would induce biases of ±50% (supporting information Figure S8).

Comparing the discharge-weighted average composition of SPM to river sediments shows that lipid biomarker proxy values are generally similar. Therefore, although investigations spanning a broader range of fluvial systems are clearly needed, sampling of river sediments may serve as a convenient means to constrain the composition of suspended matter transported by river systems, including deriving detailed molecular isotopic signatures.

Ultimately, such constraints on fluvial fluxes of source-specific biomarkers associated with SPM may serve to establish quantitative links between OM production, export, and burial at the molecular level.

Acknowledgments
This project was funded by the Swiss National Science Foundation SNF ("CAPS-LOCK" and "CAPS-LOCK2;" 200021_140850). F.P. acknowledges funding from NWO-VENI grant 863.13.016. We thank the sampling crews from both field campaigns (Björn Buggle, James Saenz, Alissa Zuijdgeest, Marilu Tavagna, Stefan Eugen Filip, Silvia Lavinia Filip, Mihai, Clayton Magill, Thomas Blattmann, and Michael Albani), Daniel Montluçon for lab support and Hannah Gies for PCGC work. Figures, tables, and equations can be found in supporting information.

References

Armijos, E., Crave, A., Espinoza, R., Fraizy, P., Dos Santos, A. L. M. R., Sampaio, F., et al. (2017). Measuring and modeling vertical gradients in suspended sediments in the Solimoes/Amazon River. *Hydrological Processes*, *31*(3), 654–667. https://doi.org/10.1002/hyp.11059

Baldock, J. A., & Skjemstad, J. O. (2000). Role of the soil matrix and minerals in protecting natural organic materials against biological attack. *Organic Geochemistry*, *31*(7–8), 697–710. https://doi.org/10.1016/S0146-6380(00)00049-8

Blair, N. E., & Aller, R. C. (2012). The fate of terrestrial organic carbon in the marine environment. *Annual Review of Marine Science*, *4*(1), 401–423. https://doi.org/10.1146/annurev-marine-120709-142717

Bouchez, J., Galy, V., Hilton, R. G., Gaillardet, J., Moreira-Turcq, P., Perez, M. A., et al. (2014). Source, transport and fluxes of Amazon River particulate organic carbon: Insights from river sediment depth-profiles. *Geochimica et Cosmochimica Acta*, *133*, 280–298. https://doi.org/10.1016/j.gca.2014.02.032

Bouchez, J., Lupker, M., Gaillardet, J., France-Lanord, C., & Maurice, L. (2011). How important is it to integrate riverine suspended sediment chemical composition with depth? Clues from Amazon River depth-profiles. *Geochimica et Cosmochimica Acta*, *75*(22), 6955–6970. https://doi.org/10.1016/j.gca.2011.08.038

Callede, J., Kosuth, P., Guyot, L. J., & Guimarães, V. S. (2000). Discharge determination by Acoustic Doppler Current Profilers (ADCP): A moving bottom error correction method and its application on the River Amazon at Obidos. *Hydrological Sciences Journal*, *45*(6), 911–924. https://doi.org/10.1080/02626660009492392

Cathalot, C., Rabouille, C., Pastor, L., Deflandre, B., Viollier, E., Buscail, R., et al. (2010). Temporal variability of carbon recycling in coastal sediments influenced by rivers: Assessing the impact of flood inputs in the Rhone River prodelta. *Biogeosciences*, *7*(3), 1187–1205.

Cathalot, C., Rabouille, C., Tisnerat-Laborde, N., Toussaint, F., Kerherve, P., Buscail, R., et al. (2013). The fate of river organic carbon in coastal areas: A study in the Rhône River delta using multiple isotopic ($d^{13}C$, D-C) and organic tracers. *Geochimica et Cosmochimica Acta*, *118*, 33–55. https://doi.org/10.1016/j.gca.2013.05.001

Chen, C. I. (1991). Unified theory on power laws for flow resistance. *Journal of Hydraulic Engineering-ASCE*, *117*(3), 371–389. https://doi.org/10.1061/(ASCE)0733-9429(1991)117:3(371)

Christl, M., Vockenhuber, C., Kubik, P. W., Wacker, L., Lachner, J., Alfimov, V., et al. (2013). The ETH Zurich AMS facilities: Performance parameters and reference materials. *Nuclear Instruments and Methods in Physics Research B*, *294*, 29–38. https://doi.org/10.1016/j.nimb.2012.03.004

Clark, K. E., Hilton, R. G., West, A. J., Robles Caceres, A., Gröcke, D. R., Marthews, T. R., et al. (2017). Erosion of organic carbon from the Andes and its effects on ecosystem carbon dioxide balance. *Journal of Geophysical Research: Biogeosciences*, *122*, 449–469. https://doi.org/10.1002/2016JG003615

De Jonge, C., Hopmans, E. C., Zell, C. I., Kim, J. H., Schouten, S., & Sinninghe Damsté, J. S. (2014a). Occurrence and abundance of 6-methyl branched glycerol dialkyl glycerol tetraethers in soils: Implications for palaeoclimate reconstruction. *Geochimica et Cosmochimica Acta*, *141*, 97–112. https://doi.org/10.1016/j.gca.2014.06.013

De Jonge, C., Stadnitskaia, A., Hopmans, E. C., Cherkashov, G., Fedotov, A., & Sinninghe Damsté, J. S. (2014b). In situ produced branched glycerol dialkyl glycerol tetraethers in suspended particulate matter from the Yenisei River, Eastern Siberia. *Geochimica et Cosmochimica Acta*, *125*, 476–491. https://doi.org/10.1016/j.gca.2013.10.031

Doetterl, S., Stevens, A., Six, J., Merckx, R., Van Oost, K., Pinto, M. C., et al. (2015). Soil carbon storage controlled by interactions between geochemistry and climate. *Nature Geoscience*, *8*(10), 780. https://doi.org/10.1038/ngeo2516

Eglinton, T. I., Aluwihare, L. I., Bauer, J. E., Druffel, E. R. M., & McNichol, A. P. (1996). Gas chromatographic isolation of individual compounds from complex matrices for radiocarbon dating. *Analytical Chemistry*, *68*(5), 904–912. https://doi.org/10.1021/ac9508513

Eglinton, T. I., & Eglinton, G. (2008). Molecular proxies for paleoclimatology. *Earth and Planetary Science Letters*, *275*(1–2), 1–16. https://doi.org/10.1016/j.epsl.2008.07.012

Feng, X. J., Feakins, S. J., Liu, Z. G., Ponton, C., Wang, R. Z., Karkabi, E., et al. (2016). Source to sink: Evolution of lignin composition in the Madre de Dios River system with connection to the Amazon basin and offshore. *Journal of Geophysical Research: Biogeosciences*, *121*, 1316–1338. https://doi.org/10.1002/2016JG003323

Freymond, C. V., Kündig, N., Stark, C., Peterse, F., Buggle, B., Lupker, M., et al. (2018). Evolution of biomolecular loadings along a major river system. *Geochimica et Cosmochimica Acta*, *223*, 389–404. https://doi.org/10.1016/j.gca.2017.12.010

Freymond, C. V., Peterse, F., Fischer, L. V., Filip, F., Giosan, L., & Eglinton, T. I. (2017). Branched GDGT signals in fluvial sediments of the Danube River basin: Method comparison and longitudinal evolution. *Organic Geochemistry*, *103*, 88–96. https://doi.org/10.1016/j.orggeochem.2016.11.002

Galy, V., France-Lanord, C., & Lartiges, B. (2008). Loading and fate of particulate organic carbon from the Himalaya to the Ganga-Brahmaputra delta. *Geochimica et Cosmochimica Acta*, *72*(7), 1767–1787. https://doi.org/10.1016/j.gca.2008.01.027

Galy, V., Peucker-Ehrenbrink, B., & Eglinton, T. I. (2015). Global carbon export from the terrestrial biosphere controlled by erosion. *Nature*, *521*(7551), 204–207. https://doi.org/10.1038/nature14400

Goni, M. A., Cathey, M. W., Kim, Y. H., & Voulgaris, G. (2005). Fluxes and sources of suspended organic matter in an estuarine turbidity maximum region during low discharge conditions. *Estuarine Coastal and Shelf Science*, *63*(4), 683–700. https://doi.org/10.1016/j.ecss.2005.01.012

GRDC (2018). UNH/GRDC Composite Runoff Fields V 1.0. Retrieved from http://www.grdc.sr.unh.edu/html/Polygons/P6742900.html, accessed 25 April 2018.

Guinoiseau, D., Bouchez, J., Gelabert, A., Louvat, P., Filizola, N., & Benedetti, M. F. (2016). The geochemical filter of large river confluences. *Chemical Geology*, *441*, 191–203. https://doi.org/10.1016/j.chemgeo.2016.08.009

Habersack, H., Hein, T., Stanica, A., Liska, I., Mair, R., Jager, E., et al. (2016). Challenges of river basin management: Current status of, and prospects for, the River Danube from a river engineering perspective. *Science of the Total Environment*, *543*, 828–845. https://doi.org/10.1016/j.scitotenv.2015.10.123

Hemingway, J. D., Schefuß, E., Spencer, R. G. M., Dinga, B. J., Eglinton, T. I., McIntyre, C., et al. (2017). Hydrologic controls on seasonal and inter-annual variability of Congo River particulate organic matter source and reservoir age. *Chemical Geology*, *466*, 454–465. https://doi.org/10.1016/j.chemgeo.2017.06.034

Hopmans, E. C., Schouten, S., & Sinninghe Damsté, J. S. (2016). The effect of improved chromatography on GDGT-based palaeoproxies. *Organic Geochemistry*, *93*, 1–6. https://doi.org/10.1016/j.orggeochem.2015.12.006

Keil, R. G., & Mayer, L. M. (2014). Mineral matrices and organic matter. In Turekian, K. K. (Ed.), *Treatise on geochemistry* (2nd ed., pp. 337–359). Oxford, UK: Elsevier. https://doi.org/10.1016/B978-0-08-095975-7.01024-X

Kusch, S., Rethemeyer, J., Schefuß, E., & Mollenhauer, G. (2010). Controls on the age of vascular plant biomarkers in Black Sea sediments. *Geochimica et Cosmochimica Acta*, *74*(24), 7031–7047. https://doi.org/10.1016/j.gca.2010.09.005

Lattaud, J., Kirkels, F., Peterse, F., Freymond, C. V., Eglinton, T. I., Hefter, J., et al. (2018). Long-chain diols in rivers: Distribution and potential biological sources. *Biogeosciences Discussions*, 1–24. https://doi.org/10.5194/bg-2018-116

Li, R. C., Fan, J., Xue, J. T., & Meyers, P. A. (2017). Effects of early diagenesis on molecular distributions and carbon isotopic compositions of leaf wax long chain biomarker n-alkanes: Comparison of two one-year-long burial experiments. *Organic Geochemistry*, *104*, 8–18. https://doi.org/10.1016/j.orggeochem.2016.11.006

Lupker, M., France-Lanord, C., Lave, J., Bouchez, J., Galy, V., Metivier, F., et al. (2011). A Rouse-based method to integrate the chemical composition of river sediments: Application to the Ganga basin. *Journal of Geophysical Research*, *116*, F04012. https://doi.org/10.1029/2010JF001947

McIntyre, C. P., Wacker, L., Haghipour, N., Blattmann, T. M., Fahrni, S., Usman, M., et al. (2016). Online ^{13}C and ^{14}C gas measurements by EA-IRMS-AMS at ETH Zürich. *Radiocarbon*, *59*, 893–903. https://doi.org/10.1017/RDC.2016.68

Milliman, J., & Farnsworth, K. (2011). *Runoff, erosion, and delivery to the coastal ocean, river discharge to the coastal ocean: A global synthesis*. Cambridge, UK: Cambridge University Press. https://doi.org/10.1017/CBO9780511781247.003

Muste, M., Yu, K., & Spasojevic, M. (2004). Practical aspects of ADCP data use for quantification of mean river flow characteristics; Part 1: Moving-vessel measurements. *Flow Measurement and Instrumentation*, *15*(1), 1–16. https://doi.org/10.1016/j.flowmeasinst.2003.09.001

Parsons, D. R., Jackson, P. R., Czuba, J. A., Engel, F. L., Rhoads, B. L., Oberg, K. A., et al. (2013). Velocity Mapping Toolbox (VMT): A processing and visualization suite for moving-vessel ADCP measurements. *Earth Surface Processes and Landforms*, *38*(11), 1244–1260. https://doi.org/10.1002/esp.3367

Peterse, F., & Eglinton, T. I. (2017). Grain size associations of branched tetraether lipids in soils and riverbank sediments: Influence of hydrodynamic sorting processes. *Frontiers in Earth Science*, *5*, 49. https://doi.org/10.3389/feart.2017.00049

Peterse, F., van der Meer, J., Schouten, S., Weijers, J. W. H., Fierer, N., Jackson, R. B., et al. (2012). Revised calibration of the MBT-CBT paleotemperature proxy based on branched tetraether membrane lipids in surface soils. *Geochimica et Cosmochimica Acta*, *96*, 215–229. https://doi.org/10.1016/j.gca.2012.08.011

R Core Team (2014). *R: A language and environment for statistical computing*. Vienna, Austria: R Foundation for Statistical Computing.

Rosenheim, B. E., Roe, K. M., Roberts, B. J., Kolker, A. S., Allison, M. A., & Johannesson, K. H. (2013). River discharge influences on particulate organic carbon age structure in the Mississippi/Atchafalaya River System. *Global Biogeochemical Cycles*, *27*, 154–166. https://doi.org/10.1002/gbc.20018

Saliot, A., Parrish, C. C., Sadouni, N., Bouloubassi, L., Fillaux, J., & Cauwet, G. (2002). Transport and fate of Danube Delta terrestrial organic matter in the Northwest Black Sea mixing zone. *Marine Chemistry*, *79*, 243–259. https://doi.org/10.1016/S0304-4203(02)00067-1

Schiller, H., Miklós, D., & Sass, J. (2010). The Danube River and its basin physical characteristics, water regime and water balance. In Mitja, B. (Ed.), *Hydrological processes of the Danube River Basin. Perspectives from the Danubian Countries* (pp. 25–77). Dordrecht, Netherlands: Springer. https://doi.org/10.1007/978-90-481-3423-6

Schouten, S., Hopmans, E. C., & Sinninghe Damsté, J. S. (2013). The organic geochemistry of glycerol dialkyl glycerol tetraether lipids: A review. *Organic Geochemistry*, *54*, 19–61. https://doi.org/10.1016/j.orggeochem.2012.09.006

Shah, S. R., & Pearson, A. (2007). Ultra-microscale (5–25 μgC) analysis of individual lipids by ^{14}C AMS: Assessment and correction for sample processing blanks. *Radiocarbon*, *49*(1), 69–82. https://doi.org/10.1017/S0033822200041904

Smith, J. C., Galy, A., Hovius, N., Tye, A. M., Turowski, J. M., & Schleppi, P. (2013). Runoff-driven export of particulate organic carbon from soil in temperate forested uplands. *Earth and Planetary Science Letters*, *365*, 198–208. https://doi.org/10.1016/j.epsl.2013.01.027

Sommerwerk, N., Hein, T., Schneider-Jacoby, M., Baumgartner, C., Ostojic, A., Sieber, R., et al. (2009). The Danube River Basin. In Tockner, K., Robinson, C. T., & Uehlinger, U. (Eds.), *Rivers of Europe* (pp. 59–112). London, UK: Elsevier Science. https://doi.org/10.1016/B978-0-12-369449-2.00022-9

Sternström, K. E., Skog, G., Georgiadou, E., Genberg, J., & Johansson, A. (2011). *A guide to radiocarbon units and calculations*. Lund, Sweden: Lund University.

Synal, H. A., Stocker, M., & Suter, M. (2007). MICADAS: A new compact radiocarbon AMS system. *Nuclear Instruments and Methods in Physics Research B*, *259*, 7–13. https://doi.org/10.1016/j.nimb.2007.01.138

Tao, S. Q., Eglinton, T. I., Montlucon, D. B., McIntyre, C., & Zhao, M. X. (2015). Pre-aged soil organic carbon as a major component of the Yellow River suspended load: Regional significance and global relevance. *Earth and Planetary Science Letters*, *414*, 77–86. https://doi.org/10.1016/j.epsl.2015.01.004

Tao, S. Q., Eglinton, T. I., Zhang, L., Yi, Z., Montlucon, D., McIntyre, C., et al. (2017). Temporal variability in composition and fluxes of Yellow River particulate organic matter. *Limnology and Oceanography: Methods*, *63*, S119–S141. https://doi.org/10.1002/lno.10727

Tierney, J. E., & Russell, J. M. (2009). Distributions of branched GDGTs in a tropical lake system: Implications for lacustrine application of the MBT/CBT paleoproxy. *Organic Geochemistry*, *40*, 1032–1036. https://doi.org/10.1016/j.orggeochem.2009.04.014

Torica, V. (2006). Physiography and climate. In Tudorancea, C. & Tudorancea, M. M. (Eds.), *Danube delta: Genesis and biodiversity*. Leiden, Netherlands: Backhuys.

Van der Voort, T. S., Zell, C. I., Hagedorn, F., Feng, X., McIntyre, C. P., Haghipour, N., et al. (2017). Diverse soil carbon dynamics expressed at the molecular level. *Geophysical Research Letters*, *44*, 11840–11850. https://doi.org/10.1002/2017GL076188

Wakeham, S. G., Canuel, E. A., Lerberg, E. J., Mason, P., Sampere, T. P., & Bianchi, T. S. (2009). Partitioning of organic matter in continental margin sediments among density fractions. *Marine Chemistry*, *115*, 211–225. https://doi.org/10.1016/j.marchem.2009.08.005

Wang, X. X., Huang, X. Y., Sachse, D., Hu, Y., Xue, J. T., & Meyers, P. A. (2016). Comparisons of lipid molecular and carbon isotopic compositions in two particle-size fractions from surface peat and their implications for lipid preservation. *Environmental Earth Sciences*, *75*, 1142. https://doi.org/10.1007/s12665-016-5960-3

Weber, Y., De Jonge, C., Rijpstra, W. I. C., Hopmans, E. C., Stadnitskaia, A., Schubert, C. J., et al. (2015). Identification and carbon isotope composition of a novel branched GDGT isomer in lake sediments: Evidence for lacustrine branched GDGT production. *Geochimica et Cosmochimica Acta*, *154*, 118–129. https://doi.org/10.1016/j.gca.2015.01.032

Weijers, J. W. H., Schouten, S., van den Donker, J. C., Hopmans, E. C., & Sinninghe Damsté, J. S. (2007). Environmental controls on bacterial tetraether membrane lipid distribution in soils. *Geochimica et Cosmochimica Acta*, *71*, 703–713. https://doi.org/10.1016/j.gca.2006.10.003

Zell, C., Kim, J. H., Balsinha, M., Dorhout, D., Fernandes, C., Baas, M., et al. (2014). Transport of branched tetraether lipids from the Tagus River basin to the coastal ocean of the Portuguese margin: Consequences for the interpretation of the MBT'/CBT paleothermometer. *Biogeosciences*, *11*, 5637–5655. https://doi.org/10.5194/bg-11-5637-2014